Journal of Solid State Chemistry 186 (2012) 247–254

Contents lists available at SciVerse ScienceDirect

Journal of Solid State Chemistry

journal homepage: www.elsevier.com/locate/jssc

Microwave-assisted hydrothermal synthesis of marigold-like $ZnIn_2S_4$ microspheres and their visible light photocatalytic activity

Zhixin Chen [a,b,*], Danzhen Li [a], Guangcan Xiao [a,b], Yunhui He [a,b], Yi-Jun Xu [a]

[a] Research Institute of Photocatalysis, State Key Laboratory Breeding Base of Photocatalysis, College of Chemistry and Chemical Engineering, Fuzhou University, Fuzhou 350002, PR China

[b] Analysis and Test Center, Fuzhou University, Fuzhou 350002, PR China

ARTICLE INFO

Article history:
Received 6 August 2011
Received in revised form
29 November 2011
Accepted 4 December 2011
Available online 9 December 2011

Keywords:
Microwave-assisted hydrothermal
$ZnIn_2S_4$
Visible
Photocatalytic activity

ABSTRACT

Marigold-like $ZnIn_2S_4$ microspheres were synthesized by a microwave-assisted hydrothermal method with the temperature ranging from 80 to 195 °C. X-ray diffraction, X-ray photoelectron spectroscopy, nitrogen sorption analysis, UV–visible spectroscopy, scanning electron microscopy and transmission electron microscopy were used to characterize the products. It was found that the crystallographic structure and optical property of the products synthesized at different temperatures were almost the same. The degradation of methyl orange (MO) under the visible light irradiation has been used as a probe reaction to investigate the photocatalytic activity of as-prepared $ZnIn_2S_4$, which shows that the $ZnIn_2S_4$ sample synthesized at 195 °C shows the best photocatalytic activity for MO degradation. In addition, the photocatalytic activities of all the samples prepared by the microwave-assisted hydrothermal method are better than those prepared by a normal hydrothermal method, which could be attributed to the formation of more defect sites during the microwave-assisted hydrothermal treatment.

1. Introduction

Nowadays, the microwave-assisted synthesis of nanostructured materials has gained popularity because the approach of microwave irradiation provides a rapid and homogeneous heating of the entire sample, enhances reaction rates and facilitates formation of uniform nucleation centers. Thus, it is energy efficient and environmentally friendly [1]. It has been realized that the microwave system provides the opportunity for completing reactions in minutes instead of spending hours or even days on synthesizing a single compound. In particular, modern microwave systems offer the capability of temperature and time programming, allowing fast and easy optimization of reaction conditions. Compared to other solution-phase synthetic methods using conventional heating methods, microwave heating techniques are potentially competitive for scale-up industrial production of high-quality nanomaterials [1–5]. All of these advantages make the microwave-assisted hydrothermal method becoming a practical application in academia and industry [6–9].

$ZnIn_2S_4$, as one of materials in the ternary chalcogenides families, has attracted widespread attention owing to its potential of application in photocatalysis [10–14]. For instance, Chen et al. has successfully synthesized $ZnIn_2S_4$ microspheres using hydrothermal method and investigated the photocatalytic degradation of dyes under the visible light irradiation [10]. Shen et al. reported that $ZnIn_2S_4$ was synthesized via a cetyltrimethyl ammonium bromide (CTAB)-assisted hydrothermal method and investigated the photocatalytic hydrogen production from water under the visible-light irradiation [11]. Fang et al. reported a solventhermal synthesis of homogeneous $ZnIn_2S_4$ nano/micropeony and examined their potential application for photodegradation of methylene blue under the irradiation of visible light [12]. Recently, hierarchically porous $ZnIn_2S_4$ submicrospheres have been synthesized by Hu et al. through a microwave-solvothermal approach and showed enhanced visible light photocatalytic activity for methylene blue degradation [15]. Despite these advances, the method as employed by Hu et al. relied on the organic solvent ethylene glycol and relatively high temperature (200 °C). Therefore, further development of the direct fabrication of $ZnIn_2S_4$ with a low temperature, template-free, facile and green synthetic method in an aqueous solution will be of much interest. In particular, to the best of our knowledge, there has been no report on the microwave-assisted hydrothermal synthesis of $ZnIn_2S_4$.

Herein, the microwave-assisted hydrothermal method was used to synthesize $ZnIn_2S_4$ with a marigold-like microstucture. A series of reaction conditions were investigated in detail, such as reaction temperatures, the pH of reaction solution, and the

* Corresponding author at: Research Institute of Photocatalysis, State Key Laboratory Breeding Base of Photocatalysis, College of Chemistry and Chemical Engineering, Fuzhou University, Fuzhou 350002, PR China. Fax: +86 591 87893206.
E-mail address: czx@fzu.edu.cn (Z. Chen).

0022-4596/$ - see front matter © 2011 Elsevier Inc. All rights reserved.
doi:10.1016/j.jssc.2011.12.006

reaction time, and so on. Furthermore, the application of $ZnIn_2S_4$ in photocatalytic degradation of MO has been investigated.

2. Experimental section

2.1. Synthesis

All chemicals were analytical grade and used as received without further purification. In a typical reaction, the ratio of $ZnCl_2$:$InCl_3$:Thioacetamide (TAA) was equal to 1:2:6. The reactants were dissolved in 50 mL water, and the pH was adjusted to 2.5 by hydrochloric acid. The 14 mL solution was transferred into the glass reaction flake with 35 mL capacity. Then, the glass flake was put into the microwave-assisted synthesis equipment (Explorer 48, CEM Co. Ltd., USA). Under the maximal power of microwave set in 200 W, the reaction glass flake was maintained at 120 °C for 10 min with the infrared for volume-independent noninvasive temperature measurement. After the reaction was completed, the flake was cooled to room temperature by an air compressor. The product was collected by centrifugation and washed with deionized water and absolute ethanol several times. The final sample was dried at 60 °C in vacuum for characterization and photocatalytic reaction. A series of reaction conditions were investigated, such as the temperature, the pH effects, the concentration of reactants, the reaction time, and so on.

2.2. Characterization

The X-ray diffraction (XRD) patterns, obtained on a Bruker D8 Advance X-ray diffractometer using Cu$K\alpha_1$ irradiation (λ=1.5406 Å), were used to identify the phase constitutions in samples. The accelerating voltage and the applied current were 40 kV and 40 mA, respectively. UV–vis diffuse reflectance spectra were obtained by a Varian cary 500 UV–vis–NIR spectrometer and were converted from reflection to absorption by the Kubelka–Munk method. The specific surface area and porosities of the samples were measured by N_2 adsorption at 77 K on Micrometritics ASAP2020 analyzer and calculated by the Brunauer–Emmett–Teller (BET) method. All the samples were degassed at 343 K overnight prior to BET measurements. The general morphology of the products was examined by scanning electron microscopy (SEM) on a JEOL JSM 6700F instrument operated at 20 kV and equipped with an energy-dispersive X-ray analyzer (Phoenix). The morphology and microstructure of the composite were further investigated by transmission electron microscopy (TEM) and high-resolution TEM (HRTEM) using a JEOL JEM 2010F microscope working at 200 kV. X-ray photoelectron spectroscopy (XPS) analysis was conducted on a Kratos Axis Ultra Spectrometer with Al$K\alpha$ radiation. The acceleration voltage of 12.5 kV and emission current of 16 mA were used.

2.3. Photocatalytic activity measurements

The photocatalytic degradation of MO was carried out in an aqueous solution at ambient temperature. Briefly, 40 mg of $ZnIn_2S_4$ was suspended in an 80 mL aqueous solution containing 10 ppm MO. The system was cooled by fan and circulating water to maintain the room temperature. Prior to irradiation, the suspension was magnetically stirred in the dark to ensure establishment of an adsorption-desorption equilibrium. The visible light source system consisted of a 300 W tungsten-halogen lamp (Philips Electronics) and a composited cutoff filters that restricted the illumination to a range of 420–800 nm. Photocatalytic degradation was monitored by measuring the absorbance of solution using a Varian Cary 50 Scan UV–vis spectrophotometer.

3. Results and discussion

First of all, the phase and crystallographic structure of temperatures series products are determined by XRD. All of the samples are synthesized in 10 min. Fig. 1 shows the XRD patterns of the as-prepared temperature series $ZnIn_2S_4$ products. The XRD patterns of all the diffraction peaks could be indexed to a hexagonal phase of $ZnIn_2S_4$, which is in agreement with the literatures [15–17] and JCPDS no. 65-2023. It is noted that the corresponding intensities and full width at half maximum (FWHM) of various diffraction peaks among the products are different in some cases. For example, the peaks of (108) and (202) are discernible when the reaction temperature exceeds 120 °C; however, these peaks can hardly be seen in 80 and 100 °C samples. For others peaks, with the enhanced reaction temperature, the corresponding intensities and FWHM values are gradually incremental and decrescent, respectively. Interestingly, all the corresponding peaks intensities of the microwave-assisted samples are almost higher than the normal hydrothermal samples (Ref. [10], Fig. 1). This phenomenon is distinct and resolved on the (006) peak. It demonstrates that higher reaction temperature renders higher intensity with narrower FWHM and the improved crystallinity. In addition, the microwave-assisted reaction time is much shorter than the normal hydrothermal method whereas the better crystallinity is obtained in the microwave-assisted hydrothermal samples. Although the hexagonal phase $ZnIn_2S_4$ could be synthesized at all of the setting temperatures, the amounts of the 80 and 100 °C samples are so small. So, the 120 °C sample is selected as typical temperature in the further investigation.

Fig. 2 shows the typical EDS pattern of as-synthesized $ZnIn_2S_4$. It indicates that the sample is composed of zinc, indium, and sulfur elements. The EDS analysis also illustrates that the atom content ratio of Zn, In and S of the as-prepared $ZnIn_2S_4$ is 1.00:1.92:4.11, which is close to the stoichiometric composition of $ZnIn_2S_4$. The XPS has been carried out for further investigation

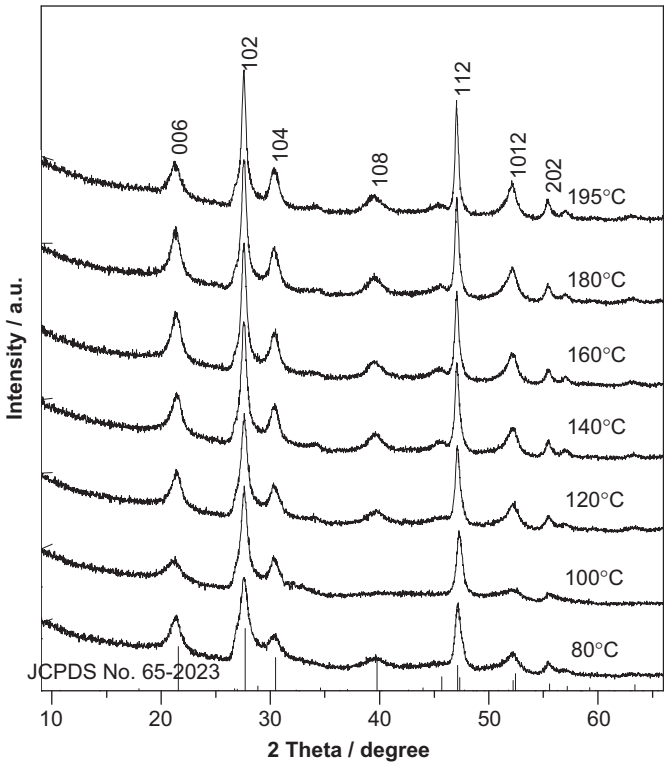

Fig. 1. XRD patterns of the as-prepared temperature series $ZnIn_2S_4$ samples.

of surface compositions and chemical states of the as-prepared $ZnIn_2S_4$ products. The results are shown in Fig. 3. As shown in Fig. 3b–d, the core lines are fixed at 1022.3 eV (Zn2*p*3/2), 445.1 eV (In3*d*5/2) and 162.0 eV (S2*p*3/2), which are corrected by referencing C 1*s* to 284.5 eV. For the In3*d*, S2*p* and Zn2*p*, the spin orbit separations (Δ) are 23.0, 7.5 and 1.2 eV, and the ratios of two peak area are 1:2, 2:3 and 1:2, respectively. These results show that the chemical states of the sample are Zn^{2+}, In^{3+} and S^{2-}, and the molar ratio of Zn:In:S is 1.0:2.1:4.1. No obvious peaks for other impurities are observed. Fig. 4 shows the UV–vis diffuse reflectance spectra of as-prepared temperature series $ZnIn_2S_4$ products. It could be seen that the temperatures series $ZnIn_2S_4$ products have similar DRS spectra. They all have a steep absorption edge in the visible range, which indicate that the relevant band gap is due

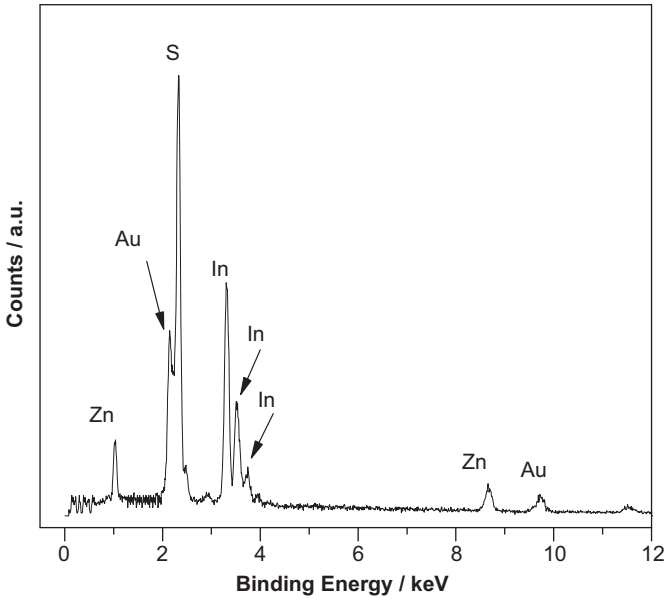

Fig. 2. Typical EDS pattern of the as-prepared $ZnIn_2S_4$ microspheres.

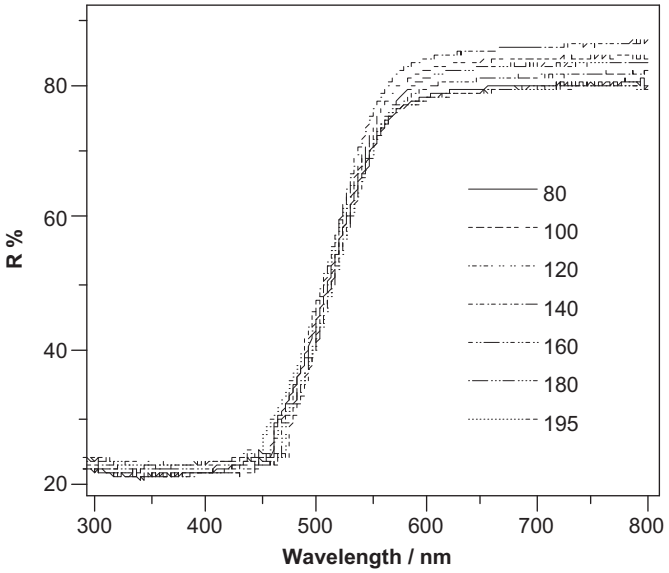

Fig. 4. DRS spectra of as-synthesized temperature series $ZnIn_2S_4$ products.

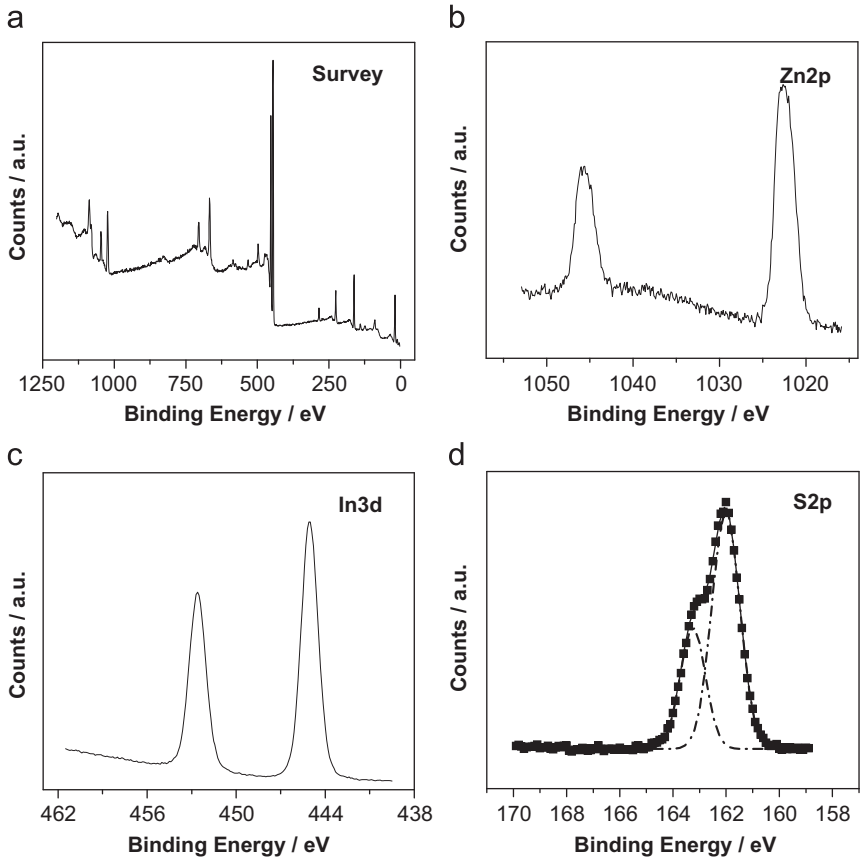

Fig. 3. XPS spectra of the as-prepared $ZnIn_2S_4$ microspheres: (a) survey; (b) Zn2*p*; (c) In3*d* and (d) S2*p*.

to the intrinsic transition of the nanomaterials rather than the transition from impurity levels [18,19]. Consequently, the as-synthesized products could be determined as pure hexagonal phase $ZnIn_2S_4$ based on the joint results of XRD, EDS, XPS and DRS characterizations.

The nitrogen adsorption–desorption isotherms of the $ZnIn_2S_4$ products are further investigated. The nitrogen adsorption and desorption isotherms are characteristic of a type IV isotherm with a hysteresis loop (Fig. 5), which indicate the presence of porous structure in the products. The S_{BET} values of the temperature series $ZnIn_2S_4$ products are enumerated in Table 1. The S_{BET} of the $ZnIn_2S_4$ products prepared at 100 °C is the lowest, 37.83 $m^2\ g^{-1}$. With the reaction temperature increasing, the data of S_{BET} are increscent. When the synthesis temperature is 195 °C, the S_{BET} is the largest, 64.79 $m^2\ g^{-1}$. The S_{BET} mutative trend of microwave-assisted samples is antithetical to the normal hydrothermal samples of our prevenient study [10]. The so-called bubbling effect maybe is the reason for this abnormal phenomenon. The microwave irradiation provides the excessive kinetic energy to the atoms or molecules. With the enhanced reaction temperature, the TAA is decomposed more quickly and drastically; then there are more bubbles generated in the synthesis system.

The morphology of the as-synthesized temperature series $ZnIn_2S_4$ is investigated by SEM. Fig. 6 shows the overall morphology of the products. Fig. 6a indicates that the $ZnIn_2S_4$ synthesize at 100 °C is composed of some microspheres whose surface nanosheets are collapsed partly. The image of the sample synthesized at 120 °C is shown in Fig. 6b. The sample is composed of a large quantity of microspheres with an average diameter of about 2 μm and have a unique marigold-like spherical superstructure which is made up of numerous nanosheets. It is similar with the $ZnIn_2S_4$ sample has been prepared at 80 °C for 6 h by hydrothermal method (Ref. [10], Fig. 3a), whereas the interspace of microwave-assisted hydrothermal samples between nanosheets is narrower and shorter than that of the normal hydrothermal samples. The reason for this phenomenon may be the high heating efficiency of microwave. Namely, the microwave irradiation approach provides a rapid and homogeneous heating of the entire sample, enhances reaction rates and facilitates formation of uniform nucleation centers. When the reaction temperature increases to 140 and 160 °C (Fig. 6c and d), there are partly microspheres joint together, and the interspaces between nanosheets are broadening. The general morphology of samples are all marigold-like microspheres. When the temperature further enhance to 180 and 195 °C (Fig. 6e and f), there are present subtotal marigold-like microspheres which sizes are about 2 μm. All in all, these results demonstrate that microwave-assisted hydrothermal process from 120 to 195 °C are all doable to synthesize the well-proportioned marigold-like microspheres composed of nanosheets, the nanosheets are collapsed incidentally when the reaction temperature is 100 °C, and the average diameter of samples does not have much difference. So, the product of 120 °C is selected for further reaction condition detailed investigation.

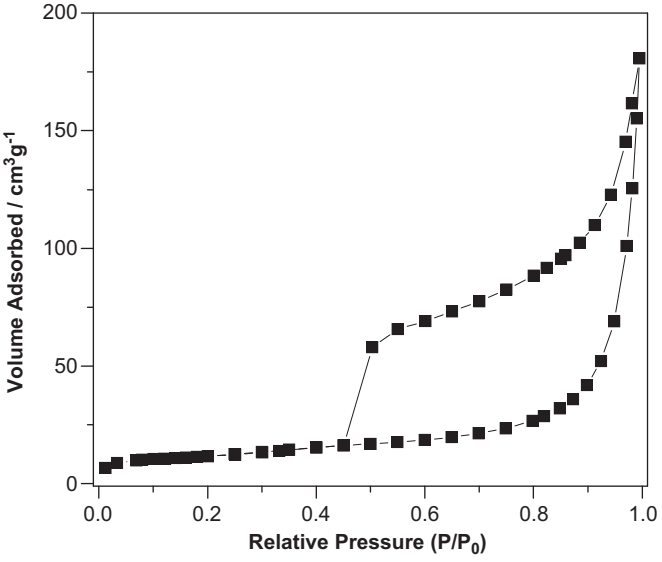

Fig. 5. The typical nitrogen adsorption-desorption isotherm of $ZnIn_2S_4$ products.

Table 1
Nitrogen adsorption–desorption isotherm results of temperature series $ZnIn_2S_4$ products.

Sample	100 °C	120 °C	140 °C	160 °C	180 °C	195 °C
$S_{BET}/m^2\ g^{-1}$	37.83	41.26	47.25	50.01	56.12	64.79

As is well known, the pH value and reaction time play important roles in determining the morphology of the products. These two factors are considered and investigated in detail. Fig. 7 displays the SEM images of the 120 °C 10 min samples prepared at pH 1 and 4. When the pH is about 4, the sample surface nanosheets are partly collapsed, as shown in Fig. 7a. However, when the pH is lower than 0.5, the solution is limpid without any precipitation. The nanosheets congeries are obtained at pH 1 (Fig. 7b), and the microsphere is gained at pH 2–3 (Fig. 6b). This phenomenon is similar with the situation of our prevenient study [16]. The reason for that would be possibly because the decomposition rate of TAA, which is correlative with the amount of TAA, the pH value of solution and the temperature of system. So the exorbitant or lower pH value is not suited for the nanosheet structure, but the moderate pH 2–3 is suitable to the formation of $ZnIn_2S_4$ microspheres. Furthermore, the SEM images of the $ZnIn_2S_4$ products prepared at 120 °C for 0.5 and 1.0 h are shown in Fig. 8. It could be seen that whether the reaction time is 0.5 h or 1.0 h, the morphology of samples are similar with the 10 min sample, and they are all well-proportioned marigold-like microspheres. So, the reaction time is not a crucial reaction condition to the regular morphology.

The product of 120 °C with reaction time of 10 min at pH 2–3 is selected for the further TEM investigation to reveal the structure of such complex microsphere. Fig. 9a presents an individual microsphere with a zigzag circle, in accordance with the SEM images (Fig. 6b). In the picture, the color of nanosheets which are vertical to the picture is dark, while the color of parallel nanosheets is light. There are some floccules between nanosheets. It may be due to the short reaction time and the faulty crystal. Fig. 9b is enlarged part of image of Fig. 9a. Clearly, some unequal nanosheets which assemble into fringes of microsphere can be seen. The selected-area electron diffraction (SAED) pattern of this part is shown in Fig. 9c. The pattern exhibits a clear hexagonal diffraction spot array and could be indexed to the single crystalline $ZnIn_2S_4$. HRTEM image is shown in Fig. 9d. The lattice interplanar spacing is measured to be 0.324 nm, corresponding to the (102) plane of hexagonal $ZnIn_2S_4$.

The visible light photocatalytic activity of $ZnIn_2S_4$ products are evaluated by degradation of MO aqueous solution. Under the visible light irradiation, the photocatalytic results of MO are shown in Fig. 10. As shown in Fig. 10, during 0–1 h, the absorption–desorption equilibrium is established after 30 min in dark. The absorption ability of these samples is similar. The 195 °C product has the maximal absorption ability which may be due to

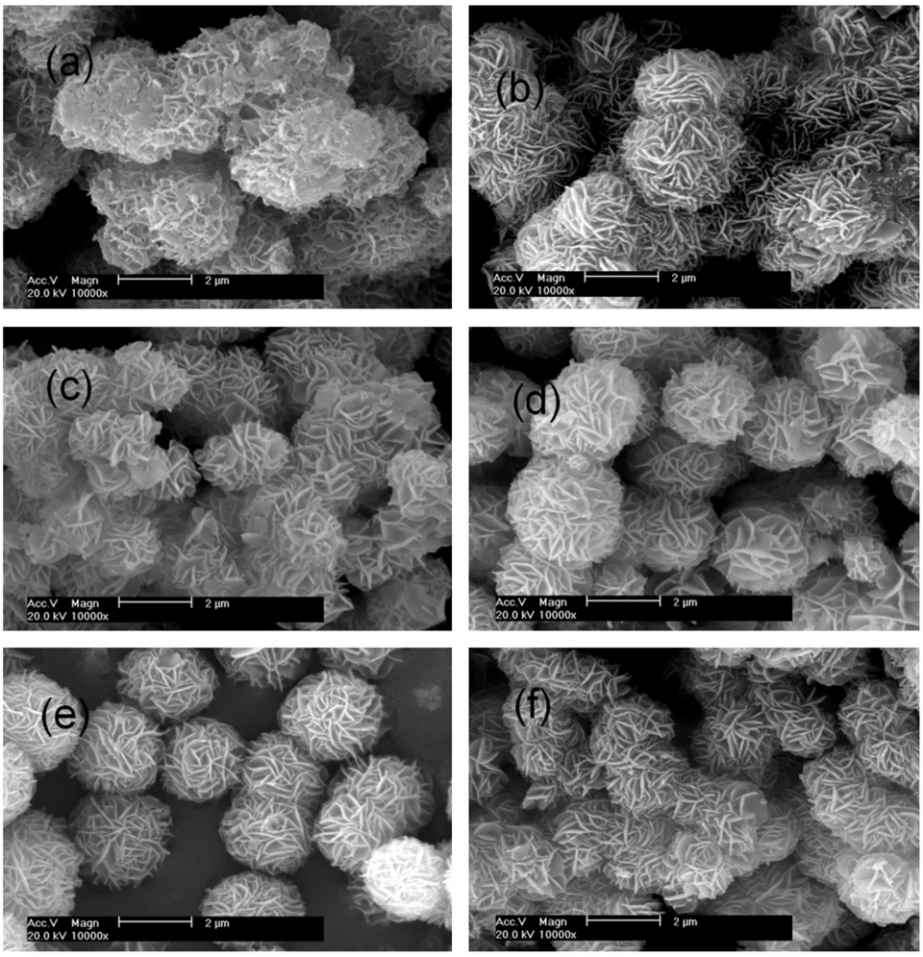

Fig. 6. SEM pictures of microwave-assisted hydrothermal synthesized temperature series of $ZnIn_2S_4$ products: (a) 100 °C, (b) 120 °C, (c) 140 °C, (d) 160 °C, (e) 180 °C and (f) 195 °C.

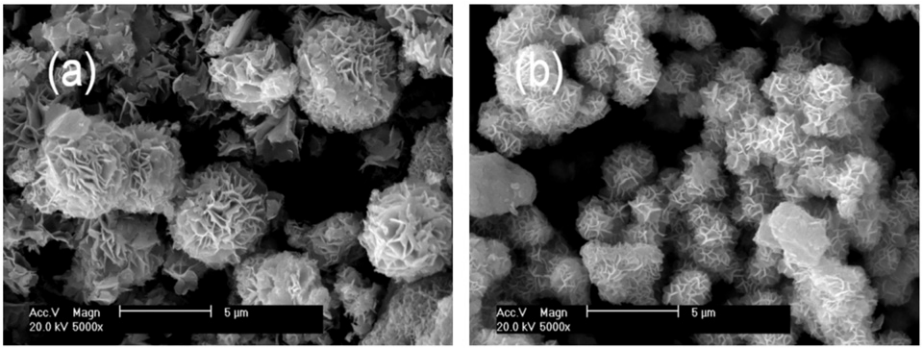

Fig. 7. SEM pictures of different pH $ZnIn_2S_4$ samples prepared at 120 °C 10 min: (a) pH 4 and (b) pH 1.

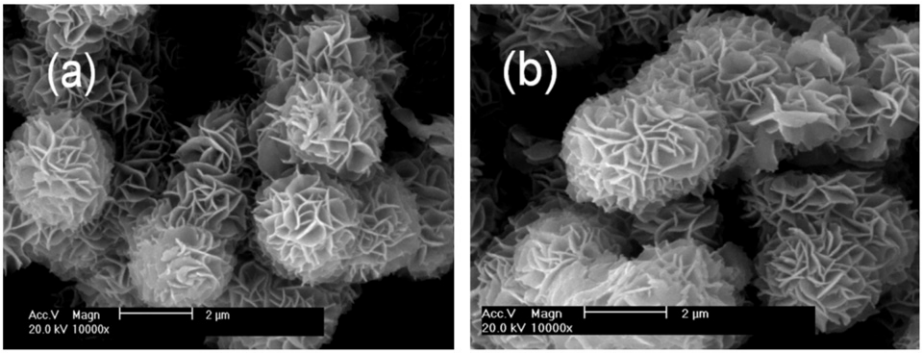

Fig. 8. SEM pictures of different hold time $ZnIn_2S_4$ samples prepared at 120 °C: (a) 0.5 h and (b) 1.0 h.

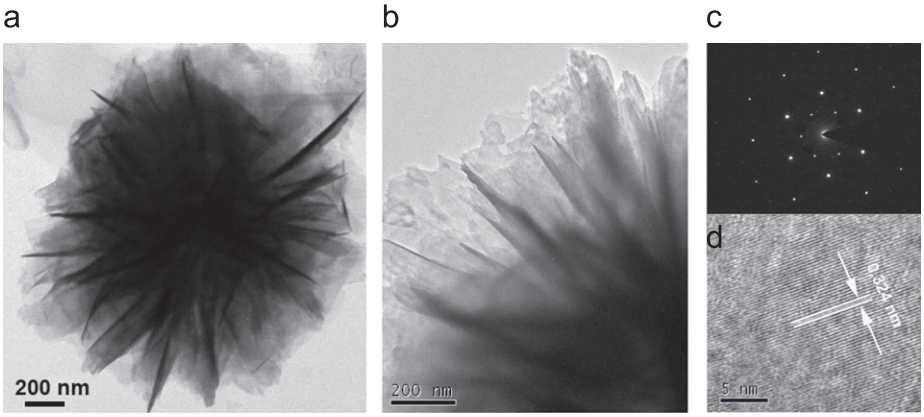

Fig. 9. (a) Low-magnification TEM, (b) high-magnification TEM, (c) selected-area electron diffraction pattern and (d) high-resolution TEM images of the synthesized $ZnIn_2S_4$.

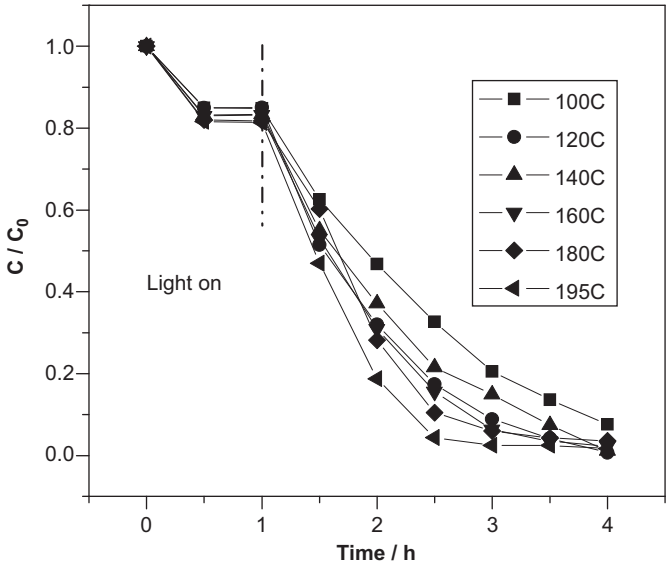

Fig. 10. Visible light photocatalytic activities of MO for the temperature series $ZnIn_2S_4$ products.

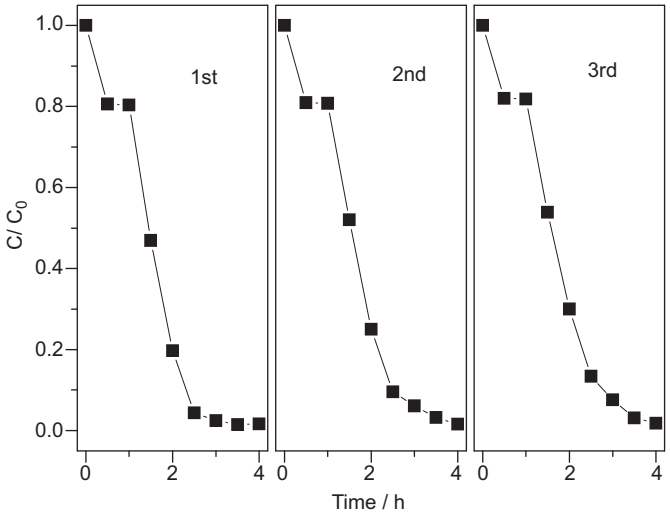

Fig. 12. Cycling runs in the photodegradation of MO in the presence of $ZnIn_2S_4$ under visible-light irradiation.

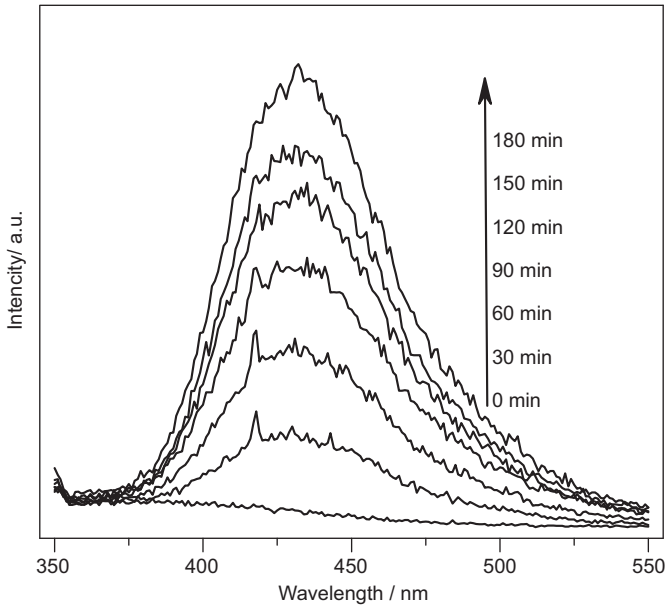

Fig. 11. OH-trapping photoluminescence spectra of $ZnIn_2S_4$ in solution of terephthalic acid at room temperature (ex, 312 nm; em, 426 nm) under visible light irradiation.

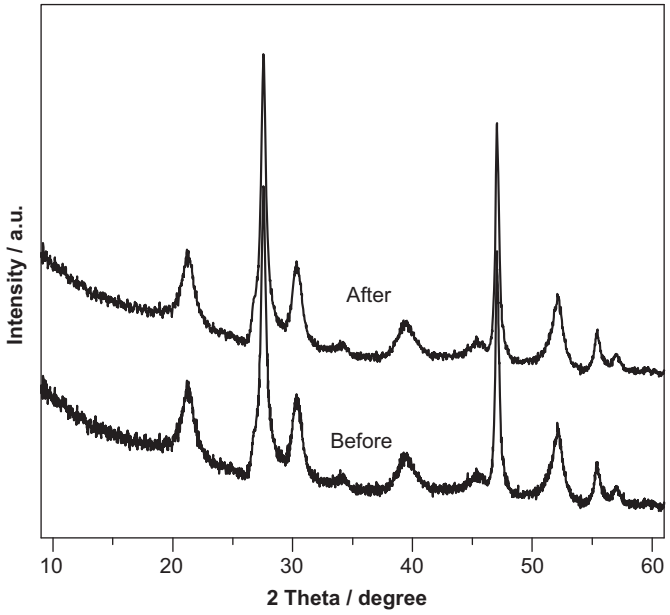

Fig. 13. Comparison of XRD patterns for $ZnIn_2S_4$ before and after reaction.

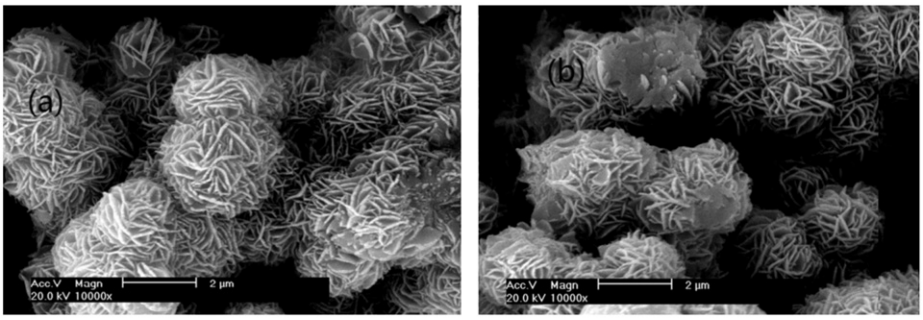

Fig. 14. Comparison of SEM pictures for $ZnIn_2S_4$ before (a) and after (b) reaction.

the largest S_{BET}, while the 100 °C product has the minimal one relevant to the least S_{BET}. Furthermore, it could be clearly seen that, as shown in Fig. 10 line 195 °C, the MO is gradually photocatalytically degraded and the 195 °C product has the best photocatalytic activity. After 2 h irradiation, the solution is nearly colorless and the value of C/C_0 is about zero. Comparison between normal and microwave-assisted samples can make us find that the photocatalytic activity of all the microwave-assisted hydrothermal samples are better than that of normal hydrothermal products (Ref. [10], Fig. 5a). The worst activity of microwave-assisted samples is the one prepared at 100 °C, it is almost the same with the best normal hydrothermal sample (80 °C). Another reason could be due to the good crystallinity obtained in the microwave-assisted hydrothermal samples, because the improvement of atomic array could create a well-order electronic configuration for improving the electron transport phenomenon that is important for photocatalytic reaction. Furthermore, work by Tichit et al. indicate that the microwave treatment probably induces higher amounts of surface defective sites than conventional treatment [20]. The surface defects serve as traps for photogenerated electrons and consequently prolong the lifetime of holes, resulting in higher photocatalytic activity. It deduce that the higher activities of microwave-assisted samples compare to the normal hydrothermal samples, may be a result of more surface defective sites due to the microwave treatment.

Fig. 11 shows the ·OH-trapping photoluminescence spectra of $ZnIn_2S_4$ in terephthalic acid solution (TAOH) at room temperature under visible light irradiation. It was evident that the active hydroxyl radicals were photogenerated on the $ZnIn_2S_4$ system under visible light irradiation. When the $ZnIn_2S_4$ system was irradiated by the visible light, the photoluminescence emission peak of TAOH (em: 426 nm) was continuously enhanced. However, when $ZnIn_2S_4$ system was in dark conditions, the fluorescence emission peak intensity of TAOH was indiscernible. In addition, the photoluminescence emission peak of TAOH cannot be detected in either dark or light system in the blank TA solution without $ZnIn_2S_4$ photocatalyst. From the above discussion, we can conclude that the large amount of •OH was generated in the $ZnIn_2S_4$ photocatalytic system under visible light irradiation. The generation of •OH plays an important role in the superior visible photocatalytic activity of the $ZnIn_2S_4$ system.

The stability of photocatalyst is important for its application. So the best photocatalyst (195 °C samples) has been selected for the stability test. Firstly, the three runs lifetime test has been done and the results are shown in Fig. 12. It indicates that the sample only exhibits slight loss of photocatalytic activity. Furthermore, the photocatalysts before and after reaction of MO have been compared by XRD and SEM investigation. Fig. 13 shows the XRD patterns of $ZnIn_2S_4$ before and after reaction. The position, intensity, and ratio of peaks are nearly the same, and no new peak is created. The SEM pictures are shown in Fig. 14. The marigold-like microspheres morphology and size are almost the same as the sample before reaction, but the nanosheets is slightly collapsed. These results suggest that the $ZnIn_2S_4$ sample are relatively stable in the MO photocatalytic reaction.

4. Conclusions

Marigold-like $ZnIn_2S_4$ microspheres are synthesized by microwave-assisted hydrothermal method from 80 to 195 °C. The optical property of temperature series products is almost the same. The microwave-assisted reaction time is much shorter than the normal hydrothermal method whereas the better crystallinity is obtained in the microwave-assisted hydrothermal samples. The S_{BET} of $ZnIn_2S_4$ microspheres increased when the synthesis temperature increased, and the largest S_{BET} is the 64.79 $m^2\,g^{-1}$ (195 °C sample). The mutative trend is opposite to the normal hydrothermal results. MO could be photocatalytically degraded by $ZnIn_2S_4$ under visible light irradiation. The $ZnIn_2S_4$ synthesized at 195 °C for 10 min show the best photocatalytic activity and relatively stable to MO degradation. The photocatalytic activity for all of the microwave-assisted hydrothermal samples is better than that of products prepared by a normal hydrothermal method. The reason may be a result of more surface defective sites formed during the microwave treatment.

Acknowledgments

This work was financially supported by the Research Program of Provincial Education Department of Fujian (0330-033064), the Scientific Development Program of Fuzhou University (826796), and the Natural Science Foundation of Fujian, China (2011J05024).

References

[1] V. Polshettiwar, M.N. Nadagouda, R.S. Varma, Aust. J. Chem. 62 (2009) 16–26.
[2] D. Dallinger, C.O. Kappe, Chem. Rev. 107 (2007) 2563–2591.
[3] J.A. Dahl, B.L.S. Maddux, J.E. Hutchison, Chem. Rev. 107 (2007) 2228–2269.
[4] J.M. Kremsner, A. Stadler, C.O. Kappe, The scale-up of microwave-assisted organic synthesis, vol. 266, 2006, pp. 233–278.
[5] B.A. Roberts, C.R. Strauss, Acc. Chem. Res. 38 (2005) 653–661.
[6] S. Yin, P. Zhnag, B. Liu, X.W. Liu, T. Sato, D.F. Xue, S.W. Lee, Res. Chem. Intermed. 36 (2010) 69–75.
[7] W.J. Li, D.Z. Li, W.J. Zhang, Y. Hu, Y.H. He, X.Z. Fu, J. Phys. Chem. C 114 (2010) 2154–2159.
[8] L. Wu, J.H. Bi, Z.H. Li, X.X. Wang, X.Z. Fu, Catal. Today 131 (2008) 15–20.
[9] S. Ribbens, V. Meynen, G. Van Tendeloo, X. Ke, M. Mertens, B.U.W. Maes, P. Cool, E.F. Vansant, Micropor. Mesopor. Mater. 114 (2008) 401–409.
[10] Z.X. Chen, D.Z. Li, W.J. Zhang, Y. Shao, T.W. Chen, M. Sun, X.Z. Fu, J. Phys. Chem. C 113 (2009) 4433–4440.
[11] S.H. Shen, L. Zhao, L.J. Guo, Int. J. Hydrogen Energy 33 (2008) 4501–4510.
[12] F. Fang, L. Chen, Y.B. Chen, L.M. Wu, J. Phys. Chem. C 114 (2010) 2393–2397.

[13] W.J. Fan, Z.F. Zhou, W.B. Xu, Z.F. Shi, F.M. Ren, H.H. Ma, S.W. Huang, Int. J. Hydrogen Energy 35 (2010) 6525–6530.
[14] P.J. Dale, K. Hoenes, J. Scragg, S. Siebentrit, Proceedings of the 34th IEEE Photovoltaic Specialists Conference (PVSC), 2009, pp. 002080–002085.
[15] X.L. Hu, J.C. Yu, J.M. Gong, Q. Li, Cryst. Growth Des. 7 (2007) 2444–2448.
[16] Z.X. Chen, D.Z. Li, W.J. Zhang, C. Chen, W.J. Li, M. Sun, Y.H. He, X.Z. Fu, Inorg. Chem. 47 (2008) 9766–9772.
[17] X.L. Gou, F.Y. Cheng, Y.H. Shi, L. Zhang, S.J. Peng, J. Chen, P.W. Shen, J. Am. Chem. Soc. 128 (2006) 7222–7229.
[18] Y.Y. Li, J.P. Liu, X.T. Huang, G.Y. Li, Cryst. Growth Des. 7 (2007) 1350–1355.
[19] J.W. Tang, Z.G. Zou, J.H. Ye, Res. Chem. Intermed. 31 (2005) 499–503.
[20] D. Tichit, A. Rolland, F. Prinetto, G. Fetter, M.D. Martinez-Ortiz, M.A. Valenzuela, P. Bosch, J. Mater. Chem. 12 (2002) 3832–3838.